Advances in Geo-Energy Research

Vol. 6, No. 5, p. 375-387, 2022

Original article

# Quantitative prediction of structural fractures in the Paleocene lower Wenchang formation reservoir of the Lufeng Depression

Hui Li[1,2], Fusheng Yu[1,2]*, Meng Wang[1,2], Yanfei Wang[3], Yilun Liu[1,2]

[1]*State Key Laboratory of Petroleum Resources and Prospecting, China University of Petroleum, Beijing 102249, P. R. China.*

[2]*College of Geosciences, China University of Petroleum, Beijing 102249, P. R. China.*

[3]*Research Institute of CNOOC China Limited, Shenzhen Branch, Shenzhen 518067, P. R. China*

**Keywords:**
Lufeng Depression
lower Wenchang formation
finite element simulation
fracture quantitative prediction

**Cited as:**
Li, H., Yu, F., Wang, M., Wang, Y., Liu, Y. Quantitative prediction of structural fractures in the Paleocene lower Wenchang formation reservoir of the Lufeng Depression. Advances in Geo-Energy Research, 2022, 6(5): 375-387.
https://doi.org/10.46690/ager.2022.05.03

**Abstract:**
Currently, the lower Paleogene Wenchang formation in the Lufeng Depression is the primary focus of reservoir development. The structural fractures that have formed inside of it not only serve as the principal path for oil migration, but also as oil storage space. As a result, the distribution features of structural fractures are crucial for future petroleum exploration and development in the Lufeng Depression. At the same time, with the quantity of conventional reservoirs in the Lufeng Depression on the decline, it is critical to determine the fracture distribution criteria for deep unconventional reservoirs. In this work, the lower Paleogene Wenchang formation in the Lufeng Depression is used as the research stratum. Then, based on existing logging data for the research region, the distinct physical properties of different rock kinds are calculated. The simulation results of the paleotectonic stress field in the study area using the finite element numerical simulation software ANSYS show that the high-value areas of maximum principal stress are the high-value areas of the uplift belt and low uplift, and the areas with low maximum principal stress are the low-value areas of Lufeng 13 Sag and the gentle slope belt in the north of Lufeng middle-low uplift. The fracture density is quantitatively predicted after the stress field simulation, which shows good agreement between the anticipated and actual observed values, and an average error of 13.61%. The predicted findings may provide new ideas for future petroleum exploration.

## 1. Introduction

Fracture refers to the natural discontinuous surface of rocks that is the result of deformation or physical diagenesis (Nelson, 2001). In general, faults and fractures both fall under the category of fractures. In a narrow sense, cracks relate primarily to microscopic fractures and minute faults. Fractures constitute important reservoir space and seepage channels; fractures in a reservoir can not only increase its permeability and porosity, but also enhance its heterogeneity, thus influencing the enrichment law and development impact of oil and gas in that reservoir. With the ongoing expansion of oil and gas exploration in China, the proportion of non-anticline reservoirs such as fractured reservoirs in oil and gas exploration is gradually on the rise. In fractured reservoirs, the degree of fracture formation has a significant effect on the productive reservoir size. Moreover, due to the complicated circumstances of fracture generation, a multiphase building campaign might readily influence the early formation of fractures (Olson et al., 2009; Baytok and Pranter, 2013; Chen et al., 2021). Researchers from all over the world, both domestic and foreign, started making predictions about reservoir fractures in the early 1920s. The majority of the applied methods included field identification, analogies, logging data, seismic attributes, and tectonic stress field prediction (Feng et al., 2018). However, the first three of these approaches require a vast quantity of fundamental geological data. For regions with limited data, the fourth technique is applicable. Simultaneously, regional tectonic stress will lead to the development of structural

Yandy Scientific Press

*Corresponding author.
*E-mail address*: lihui1995_2022@163.com (H. Li); fushengyu@cup.edu.cn (F. Yu); 17603683245@163.com (M. Wang); wangyf@cnooc.com.cn (Y. Wang); 18810357161@163.com (Y. Liu).

Received April 28, 2022; revised June 2, 2022; accepted June 20, 2022; available online June 25, 2022.

fractures on the heterogeneous rock surface, which often break preferentially along the weak layer within the rock. Therefore, the formation and development of fractures are intimately connected to the region's multi-stage tectonic movements, the magnitude and direction of the stress value, and the size of the fracture. In addition, as computer applications continue to develop, the computer modeling of paleotectonic stress during fracture formation may not only restore the distribution features of the stress field during fracture development, but also precisely and efficiently anticipate fractures (Islam et al., 2011).

The formation of reservoir cracks is governed by several geological processes, such as tectonism, diagenesis and weathering. The cracks generated under the influence of tectonic events or tectonic stress field are called structural fractures. In general, these fractures are widely developed, have long extension distance, steady occurrence, as well as great regularity and direction. The trend of fracture formation typically varies with the shift of tectonic lines. Therefore, structural fractures dominate the research of reservoir fractures. According to the mechanical characteristics, these can be separated into tensile fractures and shear fractures. The Lufeng Depression is widely regarded as potentially one of the most productive oil-rich hydrocarbon units in the Pearl River Mouth Basin (Yu et al., 2016; Liao et al., 2018). In the Lufeng Depression, the black mudstone of deep lacustrine facies of the lower Wenchang formation is an important supply of rock. A previous study indicated that the oil and gas produced in the fourth member of the Wenchang formation must be transferred through fractures as a migration route, and fractures also have a certain impact on the reservoir's transformation. (Liu et al., 2017). However, there has been a relatively limited amount of research on the internal structural fractures that are present in the Lufeng Sag, and the distribution of these fractures is not particularly well understood. In addition, few studies have focused on the internal structural fractures present in the Lufeng Sag. At the same time, because the method of prediction is limited by the number of different elements, it is necessary to find a method that is acceptable for the prediction of the distribution features of structural fractures in the Lufeng Depression.

Physical simulation and numerical simulation are currently the most widely used techniques both in China and overseas for studying the tectonic stress field. The finite element numerical simulation technology is a viable approach for modeling the tectonic stress field in terms of operability and accuracy. This approach may be integrated with the real geological conditions of the research region, and computer technology can be used to combine multiple geophysical techniques to create geological models that are not constrained by time or space (Zeng and Song, 1999). The benefits of finite element numerical simulation are realized primarily in the following areas: First, finite element numerical simulation is capable of correctly simulating the evolution of geological structures under genuine geological circumstances. Second, the software development of finite element numerical simulation with easy operation and application has essentially reached maturity, with a high simulation efficiency and a short simulation cycle. Third, the theory of finite element numerical simulation technique may utilize software with a high degree of modularity and a rather developed algorithm to produce simulation results that are infinitely near the actual value of the research region. At the same time, the simulation program can visualize simulation findings more effectively (Cui et al., 2005). Importantly, the distribution law of reservoir tectonic fractures may be estimated and quantitatively predicted based on the modeling of tectonic stress field, when paired with the actual rock fracture criterion and core fracture distribution in the research region. Consequently, the focus of this research is the lower Wenchang formation of the Paleogene in the Lufeng Depression, and the geological model is established by making use of the geological map of the lower Wenchang period and the fracture distribution map that can be found further below. ANSYS is utilized to simulate the paleotectonic stress field produced by structural cracks. This is accomplished by fitting the rock mechanical characteristics in the area using traditional logging curves, so as to ensure accuracy. After this step, it is possible to acquire the distribution features of tectonic stress that was present during the creation of structural cracks. In conclusion, the density of structural fractures in the lower Wenchang period of the research region may be quantitatively predicted by making use of the right rock fracture criteria and energy law. In this work, this was achieved by utilizing the relevant rock fracture criteria and energy law.

## 2. Geological setting

The Lufeng Depression is a Cenozoic depression located northeast of the Pearl River Mouth Basin in the northern South China Sea, with an area of about 7,760 km$^2$ (Fig. 1). The structural development of the Lufeng Depression was dominated by two episodes of differential rifting (the Wenchang and Enping periods) and subsequent thermal subsidence. During the Wenchang period, the predominant regional stress direction was NNW-SSE; however, during the Enping period, the stress field direction turned counterclockwise to become approximately S-N.

The Lufeng Depression is situated where various tectonic plates meet. Throughout the formation of the sag, several tectonic cycles have emerged (Kudrass et al., 1986; Wang et al., 2019). This phenomenon was caused by the mutual movement of plates, and the five most significant tectonic cycles were as follows: (Fig. 1) (1) Shenhu event: it developed during the end of the late Cretaceous as a result of a collision between the Pacific Plate and the Indo-Eurasian Plate, which subjected the folded basement of the Lufeng Depression to strain and extension, resulting in a series of NNE-NE faults. (2) Zhuqiong event (first episode): it consisted of rifting two sub-screens together, with T83 seismic reflection as the interface, which occurred in the late Early Eocene, and Wenchang formation deposits in the depression. (3) Zhuqiong event (second episode): it occurred at the end of the late Eocene. This tectonic movement is an inheritance movement of the Zhuqiong event (first episode). The reason is that the Pacific plate has changed from NNW subduction to NWW direction on the continental margin of South China, resulting in near S-N extension rifting. At this time, the Enping formation

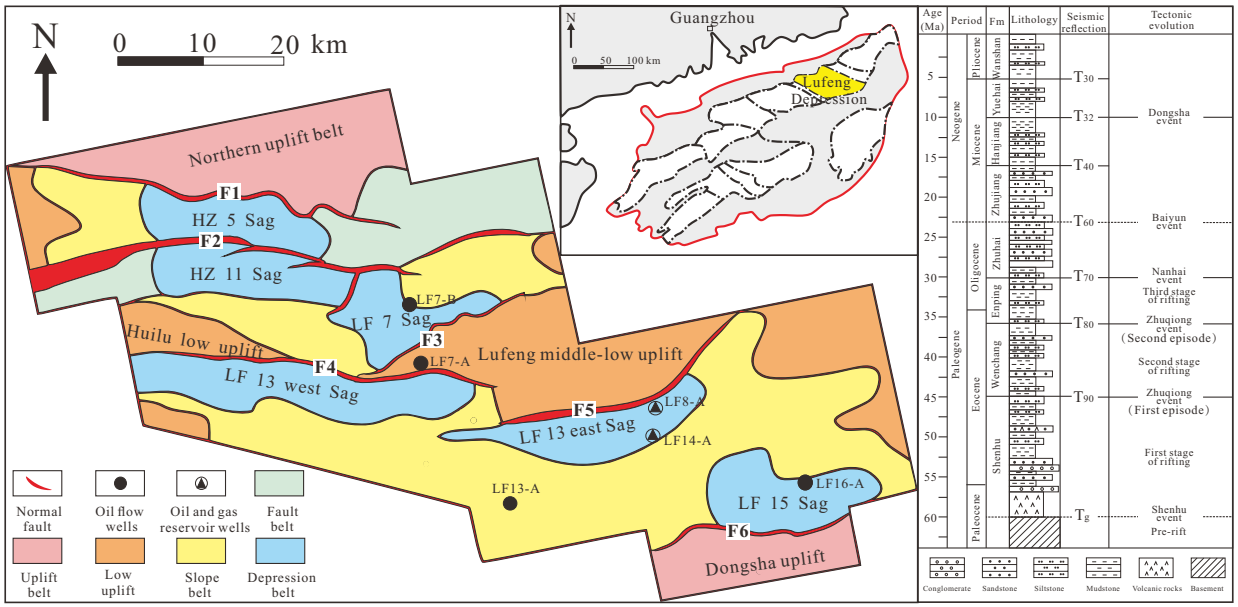


**Fig. 1**. Structural outline division and stratigraphic framework of Lufeng Depression (F1: Huizhou 5 fault, F2: Huizhou 11fault, F3: Lufeng 7 fault, F4: Lufeng 13 West Sag fault, F5: Lufeng 13 East Sag fault, F6: Lufeng 15 fault).

was deposited in the Lufeng Depression. (4) Nanhai event: it occurred in the late Oligocene, which was the longest tectonic movement in the Lufeng Depression, and then entered the depression stage. (5) Dongsha event: it took place in the late Miocene, when a series of NW-trending faults were formed. The structural pattern of the Lufeng Depression was shaped after the Dongsha event, and there was no significant change afterwards. Therefore, in the Lufeng Depression, there are two sets of rift sedimentary layers: Wenchang formation (Tg-T80) and Enping formation (T80-T70), and six sets of late rift sedimentary layers: Zhuhai formation (T70-T60), Zhujiang formation (T60-T40), Hanjiang formation (T40-T32), Yuehai Formation (T32-T30), Wanshan formation (T30-T20). The Lufeng Depression can be divided into six sags according to its internal basement properties and the regional characteristics of caprocks, which are Lufeng 15 Sag, Lufeng 7 Sag, Lufeng 13 East Sag, Lufeng 13 West Sag, Huizhou 5 Sag, and Huizhou 11 Sag (Fig. 1). The Lufeng 13 East Sag and Lufeng 15 Sag are proved to be hydrocarbon-rich sags. The distribution patterns of fault strike inside the sag are a direct manifestation of the regional stress field, and the study of the distribution characteristics of the tectonic stress field during the development of the sag is aided by the analysis of faults. The faults in the lower Wenchang phase of the Lufeng Sag are primarily separated into three groups: those with NEE, NWW, and EW trends. The NEE-trending faults are primarily developed in the middle and low uplifts and surrounding areas of Lufeng Sag, with the Lufeng 7 fault (F3) and the Lufeng 13 east fault (F5) as the main depression-controlling faults, but also including the associated secondary faults with the same trend as depression-controlling faults. The NWW-trending faults are mostly formed in the west and northwest of Lufeng Sag, primarily include the Huizhou 5 fault (F1), the Huizhou 11 fault (F2), the Lufeng 13 west fault (F4) ,and the Lufeng 15 fault (F6), and are extremely numerous in the two wings of the western Huilu low uplift. The EW-trending faults are mostly produced within the sag, apart from the sag-controlled faults. The majority are tiny secondary faults within or between strata of the same tectonic era. In general, the size of development is modest, the activity is mild, and the length of activity is brief.

## 3. Method

The existing approaches for predicting structural fractures include the rock fracture method, the major curvature method, and the energy method, among others. Both the rock fracture technique and the energy method must replicate the stress field and recover the properties of stress distribution (Rajabi, 2010). Because the majority of geological issues have several constraints, they cannot be precisely addressed. The finite element-based numerical simulation method uses basic problems to replace complex problems and solve simple problems, thereby compensating for the limitation of insufficient conditions, adapting to a variety of complex conditions, and achieving a relatively high level of calculation accuracy. Thus, it is a useful tool for analyzing the stress field. The basic idea is as follows: A complicated continuum is discretized into finite elements. The smaller the element size, the more accurate the findings. Each element mesh is allocated parameters; then, based on the boundary force conditions of the entire region, a set of equations are established and solved, where the displacement of the node is the independent variable and the stiffness matrix is the coefficient of the equations. Finally, the displacement of each node in the region is calculated by constructing an interpolation function, and the stress value of the entire region can be determined.

The rock fracture technique uses the rock fracture criterion to first examine the distribution features of the maximum

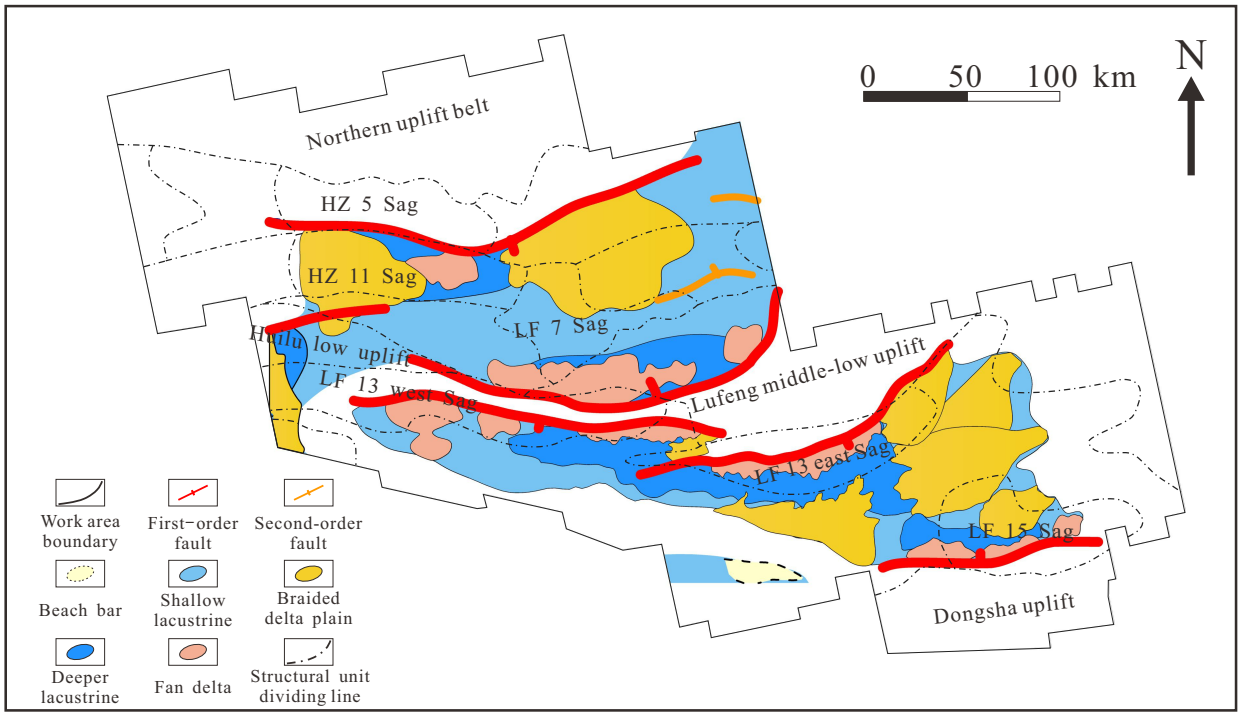


**Fig. 2**. Sedimentary facies distribution of the lower Wenchang formation in the Lufeng Depression.

principal stress, the minimum principal stress, and the shear stress in the region, and then identifies the region susceptible to brittle fracture. The acquired results are combined with the structural morphology of the area and the core-observed fracture density data to predict the fracture density distribution in the Lufeng Depression. Under the same rock thickness circumstances, a rock with higher strain capacity is more likely to form cracks than a rock with lower strain energy; thus, the crack density in a region may be predicted by calculating the rock strain energy. However, utilizing one of the approaches alone to estimate the fracture development density has shortcomings. Notwithstanding, the combination of the two strategies can mitigate the drawbacks of employing one strategy alone (Nissen et al., 2007; Wu et al., 2018).

## 4. Stress field numerical simulation

### 4.1 Geological modeling

The development of a geological model is the basis and premise of stress field simulation. When establishing the geological model's boundary, in addition to minimizing the border impact, the boundary should be perpendicular or horizontal to the major stress direction, as determined in the research region throughout the relevant epoch. This study focuses on the lower Wenchang formation in the Lufeng Depression. After examining the structural evolution features of Paleogene in the Lufeng Depression, and based on the fault distribution and sedimentary facies characteristics of the lower Wenchang formation, the finite element model (Fig. 2) is constructed. To bring the constructed geological model closer to the actual geological condition and increase the accuracy of the simulation effect, it is required to regularly alter and test the model by forwarding or inversion.

### 4.2 Parametric calculation and meshing

The selection of rock mechanics parameters is a crucial step in the finite element numerical simulation process. To simplify the model and increase the accuracy of parameter calculations, this study assigns the same physical rock parameters to the same sedimentary facies type based on a comprehensive comparison of changes in the sedimentary facies. The rock mechanics characteristics include Poisson's ratio, Young's modulus and shear modulus, among others. In general, the Poisson's ratio and Young's modulus are selected as independent parameters in the computation, and additional parameters can be determined by converting these two values. The rock strength metrics include compressive strength, tensile strength and shear strength.

Currently, the most common methods for the measurement of mechanical properties are static measurement and dynamic measurement. Rock physical analysis experiments are used to determine the deformation characteristics of rock samples under static settings. The mechanical characteristics acquired by changing and computing the speed of sound wave propagation in rocks constitute the dynamic measure. Because the standard acoustic logging data possess the features of good continuity, high longitudinal resolution and economic dependability, this study employs the dynamic technique instead of the static method to determine the rock physics parameters.

In the first phase of the stochastic modeling of rock mechanics parameters, these parameters are calculated by extracting the shear wave time difference from acoustic logging data. According to prior research (Ding et al., 1998), we use Eq. (1) to calculate the shear wave time difference:

**Table 1**. Data table of rock physical parameters of different geological bodies.

| Material code | Object | $E$ ($10^4$ MPa) | $\mu$ | $\rho$ (g/cm$^3$) |
|---|---|---|---|---|
| 1 | Shallow lacustrine | 4.58 | 0.22 | 2.37 |
| 2 | Deeper lacustrine | 2.01 | 0.38 | 2.51 |
| 3 | Braided delta plain | 2.53 | 0.35 | 2.35 |
| 4 | Fan delta | 3.25 | 0.31 | 2.68 |
| 5 | Beach bar | 3.12 | 0.29 | 2.12 |
| 6 | First-order fault | 1.80 | 0.40 | 2.30 |
| 7 | Second-order fault | 1.50 | 0.70 | 2.00 |
| 8 | Sedimentary strata | 3.00 | 0.30 | 2.10 |

$$\Delta t_s = \frac{\Delta t_p}{\left(1 - 1.15\frac{\rho^{-1}+\rho^{-3}}{e^{-\rho}}\right)} \quad (1)$$

where $\Delta t_s$ and $\Delta t_p$ denote transverse and longitudinal wave time differences, respectively, μs/ft; $\rho$ is stratum density, g/cm$^3$.

After extracting the shear wave time difference, the rock physical parameters can be calculated according to the logging data of $\rho$, $\Delta t_s$ and $\Delta t_p$. The calculation principle and equation method of the mechanical parameters of different rocks with logging data in this study are all based on the empirical statistical model between the mechanical strength parameters of related rocks and the physical quantities obtained by geophysical logging.

(1) Poisson's ratio, $\mu$

Poisson's ratio refers to the ratio of the absolute value of transverse normal strain and axial normal strain when the material is subjected to uniaxial tension or compression. The calculation equation is:

$$\mu = \frac{\Delta t_s^2 - 2\Delta t_p^2}{\Delta t_s^2 - \Delta t_p^2} \quad (2)$$

(2) Young's modulus, $E$

Young's modulus is the ratio of tensile stress to tensile strain of a material, its unit is MPa, and the relevant equation is:

$$E = \frac{\rho}{\Delta t_s^2}\frac{\Delta t_s^2 - 4\Delta t_p^2}{\Delta t_s^2 - \Delta t_p^2} \times 10^6 \quad (3)$$

(3) Shear modulus, $G$

Shear modulus is the ratio of applied stress to shear strain, its unit is MPa, and the relevant equation is:

$$G = \frac{\rho}{\Delta t_s^2} \times 10^5 \quad (4)$$

According to the above calculation equations and the logging data of the existing 20 outlet wells, $\mu$ , $E$, $G$, and other physical parameters of the rock are calculated. From the aspect of geological structure, faults not only play a crucial role in determining the shape and size of the basin, but also they serve as the connecting zones between the basin's numerous units. From the aspect of crustal deformation, the degree of fault deformation might represent the regional deformation. From the aspect of model computation outcomes, the fracture is the model's most vulnerable component (Liu et al., 2009). In this study, the fracture is divided into three grades according to scale. The fracture parameters of different grades are different, but the overall Poisson's ratio is accordingly larger than that of the surrounding rock, and the Young's modulus is 60% of the surrounding rock. Then, according to the distribution range of sedimentary facies, the average value is taken. Finally, the rock physical parameters of different sedimentary facies in the lower Wenchang period are determined (Table 1).

Using the ANSYS software tool, the 3-node triangle structure entity is utilized to mesh the research region after calculating the physical properties of various rocks. It is required to evaluate the differences between geological types during the meshing process, to group rock types with similar physical qualities into the same units, and to prevent the issue of too great meshing angle. The meshing edge length is normally determined by the unit that requires the most precise meshing. In general, the first meshing is the shortest, followed by successive divisions of the remaining entities. Eventually, 44,012 mesh units are obtained (Fig. 3).

## 4.3 Principle of stress field recovery

### 4.3.1 The key period of structural fracture formation in the lower Wenchang period

The formation of two episodes of rifting during the Paleogene in the Lufeng Depression was controlled by different regional dynamic conditions of the sedimentary period from the Wenchang formation to the Enping formation, which resulted in differences in the fault activity characteristics and stress field direction. During the sedimentary epoch of the Wenchang formation, the NW-SE tensile stress field acted upon the NE-trending faults, making them pronounced. During this period, the stress direction also dictated the formation, orientation and incidence of fractures, among other development factors (Gale et al., 2014).

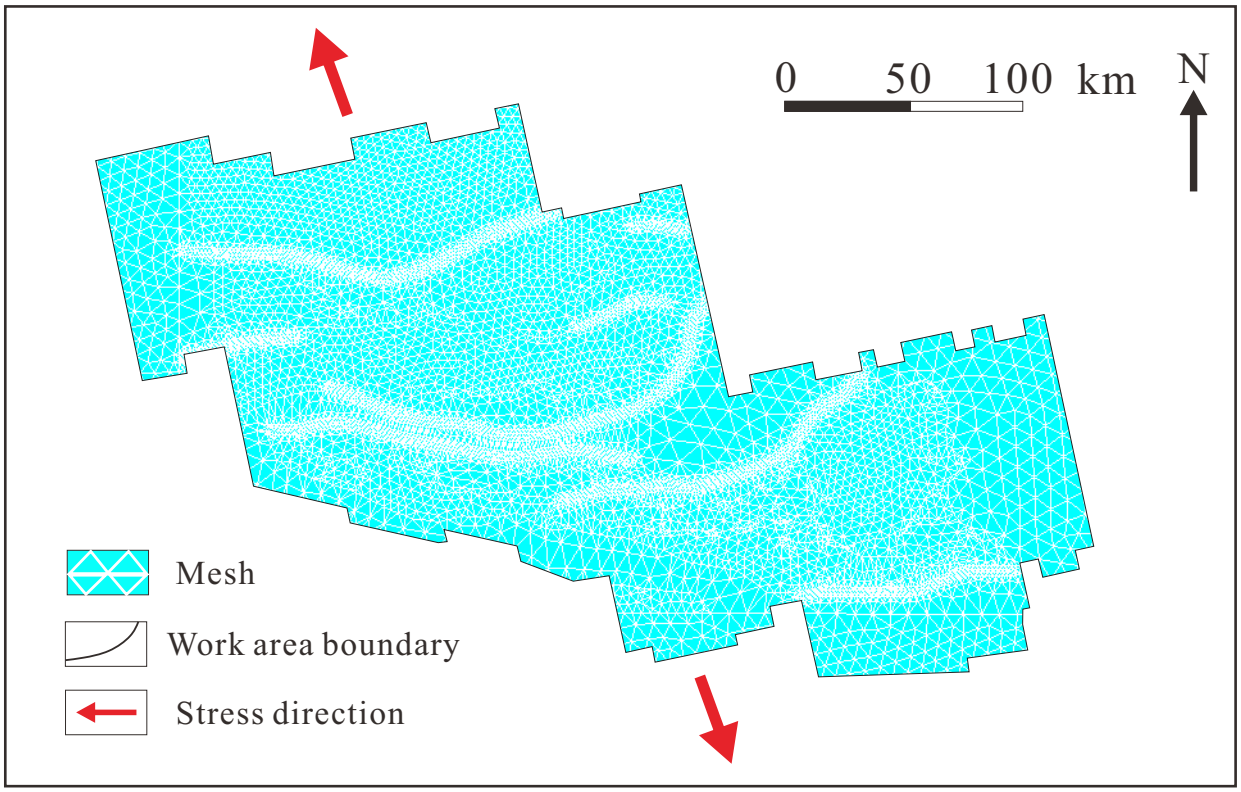


**Fig. 3**. Plane graph of meshing.

#### *4.3.2 Factors influencing the structure of reservoir fractures*

(1) Lithology: it is the most fundamental element influencing the formation of structural fractures. The lithology parameters include rock composition, particle size and density. Due to the various manifestations of each component, the mechanical characteristics of various rocks are different. Consequently, when tectonic stress circumstances are the same, the degree of structural fracture development varies. In general, the higher the percentage of brittle minerals, the finer the particles and the smaller the pore volume of rock, and the greater the development degree of structural fractures in rock under the same other conditions. (2) Structure: it is an important component influencing structural fractures. It frequently influences the formation of structural fractures by regulating the local stress distribution in various components. Due to the stress disturbance generated by fault activity, there will be a visible stress concentration along the fault zone close to the fault, and the occurrence of structural fractures will be more prevalent. Simultaneously, fractures frequently occur at the end of the fault, inflection point, and cross sections. (3) Rock mechanical characteristics: these are the primary determinants of structural fracture formation. Fragile rock or drier rock is prone to fracture deformation and fracture, but ductile rock or softer rock is more liable to plastic deformation, via the rock's internal large strain to influence the total strain, so that the development of structural cracks will be weak. (4) Stress. Tectonic fracture is the result of fracture deformation caused by regional tectonic stress; thus, the degree of tectonic fracture development is highly connected to the stress condition and rock size. The larger the stress on the rock with the other parameters being the same, the greater the degree of structural cracking in the rock. In contrast, the lower the stress on the rock, the less likely structural fissures will form in it.

#### *4.3.3 Determination of the direction of structural stress and the magnitude of paleo-stress during the formation of structural fractures*

During the Paleocene, the entire Lufeng Depression was in the area of release from the severe compressive stress of the Indo-Australian plate and Eurasian plate. In this period, the subduction rate of the Pacific plate slowed down and the subduction zone retreated, resulting in the shift of the Lufeng Depression from a compressive environment to an extension environment along the NNW-SSE direction. The boundary faults were predominantly NEE trending, generating an uplift and depression zone going NE-NEE (Westaway et al., 2002; Ross et al., 2004). By recognizing and counting the fractures in the image logging data of the known wells in the Lufeng Depression, the stress direction features of the regional stress field may be determined (Liu et al., 2022). The majority of the imaging logging data utilized in this investigation was obtained by Schlumberger's Formation MicroScanner Image (FMI). On the basis of FMI imaging log findings, the following types of fractures were often identifiable: (1) High-conductivity fracture. This is the most common fracture type in the formation, because the natural fracture fills the mud filtrate

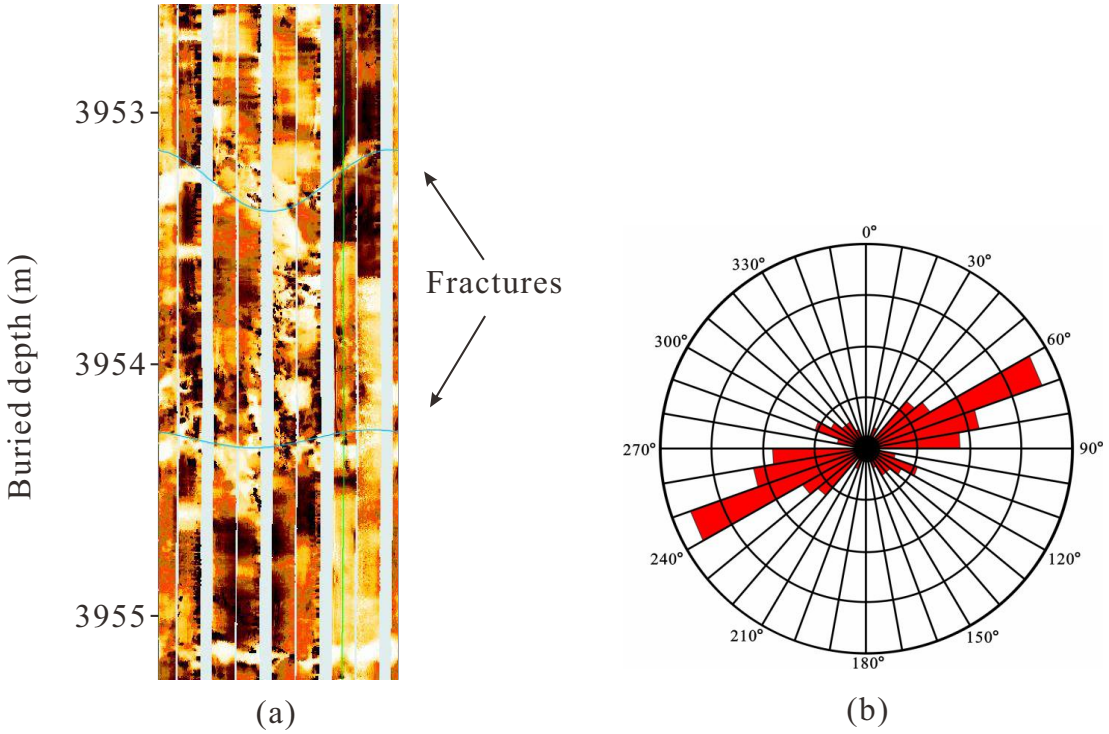


**Fig. 4**. LF14-A imaging logging (a) and rose diagram of fracture strike (b) in the Lufeng Depression.

produced by the drilling process, which is displayed on the FMI image by a dark sine curve. (2) High-resistance seam. It is filled with quartz and other minerals in the formation process, displaying a bright sinusoidal curve on the FMI image. (3) Low-conductivity fracture. This is the most common fracture type in the formation, because it is a natural fracture. (4) Fracture produced by drilling. This type of fracture is created by artificial forces, and the most distinctive of this kind is the fracture induced by the vibration of the drilling tool during drilling, which typically appears symmetrically on FMI images.

The LF14-A well is located in the eastern block of the Lufeng 13 structural belt in the Lufeng Depression. It is a complicated fault nose structure governed by an east-to-west-to-north fault in the fault rising plate. The lower Wenchang formation contains the primary oil layers in the middle and lower portions of the Wenchang formation. Multiple faults divide the Wenchang formation's structure into several blocks. The Wenchang formation contains a wide trap area. In the 3,866.0-3,960.0 m and 4,078.0-4,107.0 m portions of the LF14-A well, cracks were detected (Fig. 4(a)). Then, the fracture trend diagram of the lower Wenchang era was constructed (Fig. 4(b)). From the fracture trend rose diagram, it can be deduced that the fracture development era in the Lufeng Depression is primarily separated into two phases. Under the influence of the NNW-SSE extension stress, fractures with a NEE-SWW orientation were generated in the lower Wenchang formation.

The maximal compressive stress sustained by rocks may be measured using the acoustic emission Kaiser effect experiment (Lavrov, 2003). According to the in-situ stress measurements performed previously in the Lufeng Depression (Chen et al., 2014), the highest and minimum primary stresses during the sedimentary era of the lower Wenchang formation are 10 MPa and 2 MPa, respectively. The gravitational force on the stratum is derived from the density of the rock and the acceleration of gravity, which may be calculated automatically using the ANSYS program.

Horizontal tectonic stress is the load sustained by the geological model produced in this work, and the boundary constraint conditions are derived based on the real environment of the Lufeng Depression over different time periods. The geological model's depth direction is denoted by the $Z$-axis, which is vertically positive. The model's $X$-direction points to the positive east, while its $Y$-direction points to the positive south. The entire model may move horizontally and is constrained along the $Z$-axis. The horizontal tectonic stress is supplied to two sides of the model, while displacement constraints are imposed on the remaining two sides. In other words, the model's upper surface can move freely in the horizontal direction without stiff translation and rotation. The model is repeatedly solved until simulation results are produced that satisfy the requirements.

### 4.4 Simulation results

This study focuses primarily on the ANSYS simulation findings for maximum principal stress, minimum principal stress, and shear stress analysis. The primary causes of the aforementioned outcomes are the following: The maximum principal stress and the lowest principal stress are the main determinants of the deformation of a geological structure,

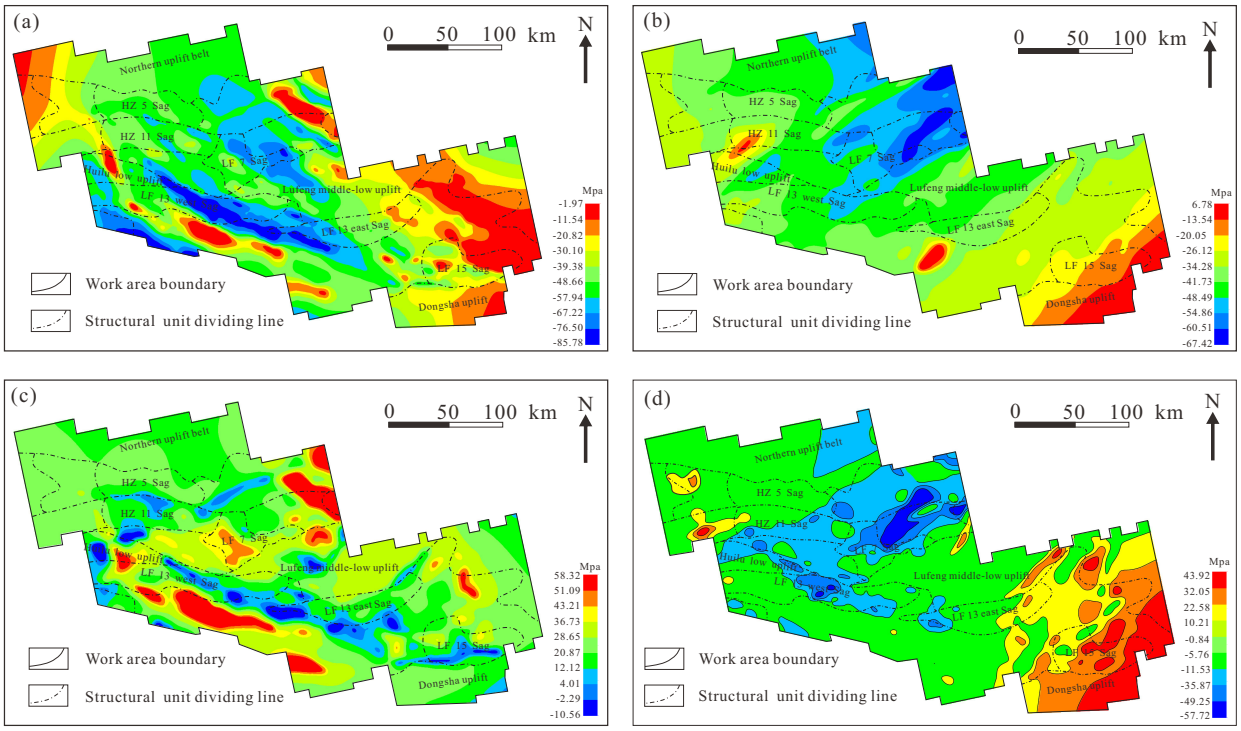


**Fig. 5**. Plane distribution characteristics of (a) maximum principal stress, (b) minimum principal stress, (c) shear stress, and (d) average stress intensity in lower Wenchang period of Lufeng Depression.

whereas shear stress plays a crucial role in regulating the creation of the fault zone. The maximum principal stress, lowest principal stress, and shear stress are all horizontal stresses described in this study. Since the geological model is influenced by extensional stress over the research period, the imposed boundary load is tensile stress. Consequently, the predominant stress in the observed data is also tensile. The positive and negative signs before the stress value do not indicate the positive and negative values of the stress, but rather its nature; the negative number indicates tensile stress, whereas the positive value indicates compressive stress. There are two types of shear stress in the acquired results: left-handed and right-handed.

The former is denoted by a positive value, while the latter by a negative value. Based on the finite element simulation results (Fig. 5), the maximum principal stress distribution range is 1.97-85.78 Mpa (Fig. 5(a)), the minimum principal stress distribution range is 6.78-67.42 Mpa (Fig. 5(b)), the shear stress distribution range is 2.29-58.32 Mpa (Fig. 5(c)) and the average stress varies between 0.84 and 57.72 Mpa (Fig. 5(d)). The highest primary stress is predominantly northwest-southeast, which is compatible with the major stress direction of the lower Wenchang formation inside the Lufeng Depression. The maximum primary stress is centered mostly in the Huilu low uplift and the Lufeng middle-low uplift. In the depression, the maximum principle stress value is very low, and the comparatively high area of the maximum principal stress in the depression is the Lufeng 15 Sag. The minimal major stress direction is predominantly east-west. The low-value area of the horizontal minimum primary stress is mostly located in the northeast Lufeng 7 Sag and the surrounding area, whereas the high-value area is primarily located in the southern Lufeng 15 Sag and the Dongsha uplift. According to the modeling results, the shear stress distribution is less impacted by faults.

## 5. Discussion

### 5.1 Quantitative prediction method of fracture

In general, tensile and shear cracks are types of cracks caused by rock fractures (Aydin, 2014). Tensile tension is the primary cause of tensile fracture, and its key features are as follows: the surface of the fracture is rough and uneven, spherical particles are prevalent, the extension distance of the entire tensile fracture is short, and the two walls are open, making it simple for some minerals to fill them. Shear fracture is a type of fracture caused by rock sliding under the effect of shear force. Its primary features are as follows: the fracture surface is generally smooth, there is a rare particle phenomenon, the extension distance of the entire shear fracture is substantial, and the termination of the fracture is prone to bifurcation (Laurent and Frantz, 2006).

Griffith's tensile fracture criterion is an equivalent maximum tensile stress theory, which can be used to determine the development degree of extended fractures. For shear fracture, the Coulomb-Moore criterion is used here. The premise is that rock fracture is the result of shear stress failure. When a shear fracture occurs, the shear stress of rock meets the Coulomb-Moore criterion.

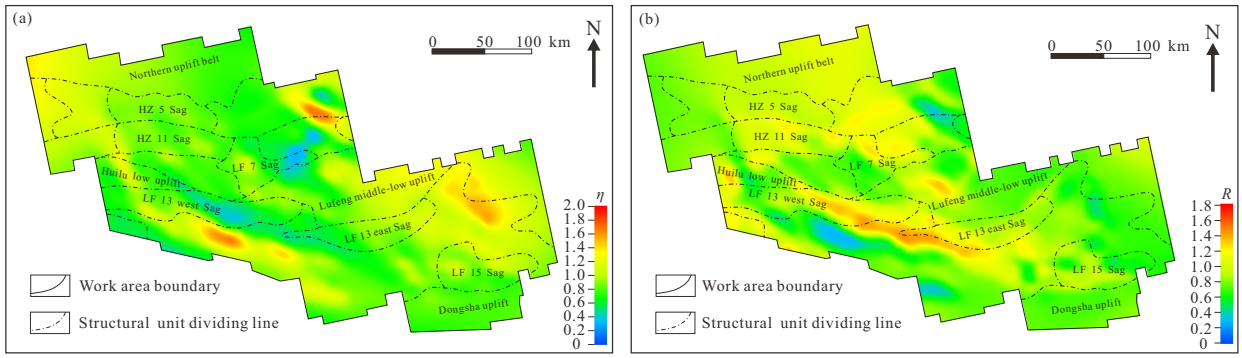


**Fig. 6**. Distribution of (a) tensile fracture development rate and (b) shear fracture development rate in lower Wenchang Formation of Lufeng Depression.

### 5.1.1 Three-dimensional Griffith fracture criterion

According to Griffith's tensile fracture criterion, when exposed to a specific stress, brittle materials with a high number of fractures will generate a concentration of tangential tensile stress around the crack. Once the tangential stress towards the end of the crack becomes strongly concentrated and its value approaches the cohesion strength of molecules in the material, brittle fracture will occur at this location. The three-dimensional axial stress of this criterion must satisfy the following:

(1) When $\sigma_1 + \sigma_3 \geq 0$:

$$\sigma_T = \frac{(\sigma_1 - \sigma_2)^2 + (\sigma_1 - \sigma_3)^2 + (\sigma_3 - \sigma_2)^2}{24(\sigma_1 + \sigma_2 + \sigma_3)} \tag{5}$$

where $\sigma_1$ denotes the horizontal maximum principal stress, MPa; $\sigma_2$ denotes the vertical principal stress, MPa; $\sigma_3$ denotes the horizontal minimum principal stress, MPa; $\sigma_T$ denotes the tensile strength of rock uniaxial tension, MPa. If $\sigma_T$ is greater than or equal to the tensile strength of the rock itself, fracture occurs.

(2) When $\sigma_1 + \sigma_3 < 0$, Griffith's fracture criterion is expressed as:

$$\sigma_T = -\sigma_3 \tag{6}$$

In summary, the tensile fracture coefficient can be indicated as:

$$\eta = \frac{\sigma_T}{\sigma_{Tc}} \tag{7}$$

where $\eta$ denotes the tensile fracture coefficient, which is dimensionless; $\sigma_{Tc}$ is the stretched fracture strength of rock, MPa, which can be measured by experiments.

### 5.1.2 Coulomb-Moore shear fracture criterion

According to the Coulomb-Moore shear fracture criterion, when the rock ruptures, there is a relationship with the normal stress $\sigma_n$ on the section. The relationship between normal stress $\sigma_n$ and shear stress $\tau_n$ can be expressed as:

$$\tau_n = C + \sigma_n \tan\varphi \tag{8}$$

where $C$ denotes the shear strength of rock, MPa; $\varphi$ is the internal friction angle of rock, rad. These two parameters are acquired from experiments or related data. When Eq. (8) is established, the rock shear fracture occurs. The shear fracture coefficient can be expressed as:

$$R = \frac{0.5(\sigma_1 - \sigma_3) + 0.5(\sigma_1 + \sigma_3)\sin\varphi}{C\cos\varphi} \tag{9}$$

where $R$ denotes the shear failure coefficient of the rock, which is dimensionless. When $R \geq 1$, the rock suffers shear failure.

The maximum and the lowest stress values of each element node may be acquired by numerical simulation for the Lufeng Depression, and the distribution of tensile fracture and shear fracture in the Lufeng Depression can be determined by applying the aforementioned fracture criterion (Fig. 6).

However, using the Griffith fracture criteria and Column-Moore shear fracture criterion, one can only assess qualitatively whether a rock fracture exists; quantitative characteristics cannot reliably forecast the fracture progression. In reality, the rock in the reservoir frequently develops both tensile and shear cracks at the same time. After comprehensive consideration, the formation fracture evaluation index $F_y$ is introduced as the comprehensive index of fracture development (Cui et al., 2009). The calculation equation is defined as:

$$F_y = a\eta + bR \tag{10}$$

where $a$ and $b$ denote the ratios of stretched and shear fractures to the total number of fractures, respectively, determined by identifying the ratios of tensile and shear fractures to the total number of fractures.

Through the proportion of tensile fractures and shear fractures in the core and imaging logging in the study area, the contribution rates of $a$ and $b$ are determined as 46.13% and 53.87%, respectively. Therefore, $F_y$ can be expressed as:

$$F_y = 0.4613\eta + 0.5387R \tag{11}$$

When $F_y \geq 1$, the rock stress has reached the fracture state. The larger the $F_y$ value, the more cracks are developed. When $F_y < 1$, the stress in the rock does not reach the fractured state, and the cracks do not develop.

**Table 2**. Error analysis between the actual statistical fracture density and the predicted fracture density.

| Well name | Actual fracture density (strip/m) | Predicted fracture density (strip/m) | Absolute error (strip/m) | Relative error (%) |
|---|---|---|---|---|
| LF7-A | 0.1057 | 0.1262 | 0.0205 | 19.39 |
| LF7-B | 0.0732 | 0.0816 | 0.0084 | 11.48 |
| LF8-A | 0.1371 | 0.1673 | 0.0302 | 22.03 |
| LF13-A | 0.0885 | 0.0794 | 0.0091 | 13.41 |
| LF14-A | 0.1304 | 0.1431 | 0.0127 | 9.74 |
| LF16-A | 0.0503 | 0.0476 | 0.0028 | 5.56 |

## 5.2 Rock deformation energy

According to prior research, the degree of fracture growth is not only proportional to the rock fracture rate, but also to the accumulated strain energy in the rock (Price, 1966). The unit volume of strain energy can be expressed by the maximum and minimum principal stresses:

$$W = \frac{\sigma_1^2 + \sigma_3^2}{2E} - \frac{\sigma_1 \sigma_3 \mu}{2E} \tag{12}$$

where $W$ denotes the strain energy, J.

The strain energy inside the rock can well reflect the development degree of structural fractures in a region, which makes up for not using the formation fracture index $F_y$ alone to predict the fracture development.

## 5.3 Fracture density prediction results

Due to the application of either formation fracture evaluation index $F_y$ or energy value $W$, these methods to predict formation fracture density $\beta$ have certain deficiencies and limitations (Ding et al., 1998). The present study predicts the development range and density of structural fractures over the sedimentary era in the Lufeng Depression by integrating the fracture value and the energy value. The appropriate equation is:

$$\beta = A_1 F_y^2 + A_2 W^2 + A_3 F_y + A_4 W + A_5 \quad (F_y \geq 1) \tag{13}$$

$$\beta = A_1 F_y^2 + A_2 F_y + A_3 \quad (F_y < 1) \tag{14}$$

where $\beta$ denotes the predicted value of fracture density, strip/m; $A_1$, $A_2$, $A_3$, $A_4$ and $A_5$ are proportional coefficients, which are based on single excellent fracture density data for the Lufeng Depression, which are fitted using the linear regression approach. The aforementioned relationship is fitted by using the core observation data and imaging logging data in Lufeng Depression, and the value of the proportionate coefficient is obtained. Finally, the quantitative fracture prediction equation for the lower Wenchang formation in the Lufeng Depression is given as:

$$\begin{aligned} \beta =& 0.00146 F_y^2 + 0.14723 W^2 - 0.0083 F_y \\ & - 0.0315 W + 0.0138 \quad (F_y \geq 1) \end{aligned} \tag{15}$$

$$\beta = 0.01652 F_y^2 - 0.017432 F_y + 0.019431 \quad (F_y < 1) \tag{16}$$

According to the above equations, fracture prediction and comparison were carried out for six wells such as LF7-A in the Lufeng Depression (Table 2). The comparative results show that the error range between the predicted fracture density and the actual statistical value is 5.5%-22.03%, and the average error is 13.61%.

Subsequently, the quantitative fracture prediction of the lower Wenchang formation in the Lufeng Depression was carried out by using Eqs. (15) and (16) (Fig. 7(a)). The results indicated that there are three regions with a higher density of structural fractures: the slope zone to the north of Lufeng 7 Sag, the Lufeng middle-low uplift to the north and east of Lufeng 13 Sag, and the low uplift to the northwest of Dongsha Uplift. The fracture density can reach 0.18 strip/m, and the fracture density isolines in these regions are dense, showing that the fracture density varies drastically across the plane, possibly due to the heterogeneity of the rock or the complicated structural properties of the region. Establishing the reasons for the stress concentration requires further research. Moreover, the middle-low uplifts near the Lufeng 7 Sag, the southwest of the research region, and the slope belt in the northwest of Lufeng 15 Sag, which are all low uplifts or uplift zones, have the most developed fractures, with a fracture density of 0.12 strip/m. In general, the fracture density in the studied region is concentrated in the range of 0.04 to 0.10 strip/m, whereas the fracture density in the majority of other places is low, ranging from 0.01 to 0.04 strip/m.

For oil and gas wells, output is frequently correlated with the success of the drilled reservoir fractures, including fracture filling, connectivity, external fluid pressure, and other variables. If the cracks near the well are not filled and have strong connection, it is likely that the well will have a high production rate, and vice versa. The fracture density prediction grade is subdivided based on the fracture development density at the lower Wenchang period in the Lufeng Depression. Therefore, the fracture development density in 0-0.06 strip/m is defined as being in an area with a grade III level of fracture development; the fracture development density in 0.06-0.13 strip/m is defined as being in an area with a grade II level of fracture development; and the fracture development density of 0.13-0.20 strip/m is defined as being in an area with a grade I level of fracture development.

Lufeng 15 sag, Lufeng 13 east sag, Lufeng 13 west gentle slope zone, Huizhou 5 east sag, and Lufeng 7 south low uplift

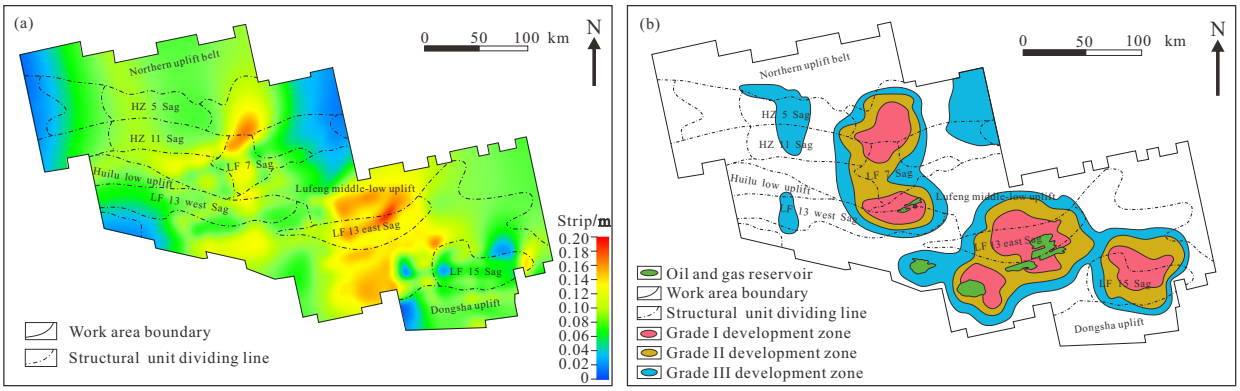


**Fig. 7**. (a) Fracture density prediction and (b) classification of fracture density for the lower Wenchang formation in the Lufeng Depression.

region are the five major locations in the predicted area for grade I fracture development, based on the Lufeng sag fracture density grade map (Fig. 7(b)). The prediction region for grade II fracture development is predominantly dispersed in blocks and is located on the periphery of the prediction area for grade I fracture development. The prognosis area for grade III fracture development is not only dispersed along the perimeter of the forecast area for grade II fracture development, but also in other regions, such as Huizhou 5 sag and Huizhou 11 middle sag, Lufeng 13 west sag, and the southwest gentle slope zone. By superimposing the fracture density prediction grade diagram with the proven Wenchang oil reservoirs in the Paleogene Lufeng Depression, it was discovered that the oil reservoirs are primarily distributed in the east of Lufeng 13 Sag and the Lufeng 7 Sag, as well as the middle-low uplift in the south and the gentle slope belt in the southwest. Also, the distribution range of known oil reservoirs coincides with the area with high fracture density.

### 5.4 Test of prediction results

After analyzing the predicted fracture density and the oil reserves of the known wells in the Lufeng Depression, it was determined that the predicted fracture density is positively correlated with the oil reserves of the known wells in the Lufeng Depression (Fig. 8), and the $R^2$ is 0.7199, indicating that the correlation between the two is very strong, and the oil reserves in the regions with relatively developed fractures are also abundant. In addition, this result demonstrates the viability of the quantitative fracture prediction approach used in this study and the reliability of the prediction outcomes.

## 6. Conclusions

1) The fractures that occurred in the lower Wenchang formation of the Lufeng Depression are mostly structural fractures that were primarily controlled by the NW-SE extension stress field during the early Paleogene. The maximal primary stress direction for the production of structural fractures is approximately 340° NNE.
2) Depending on the simulation results of the finite element stress field, there are three high-value areas of maximum

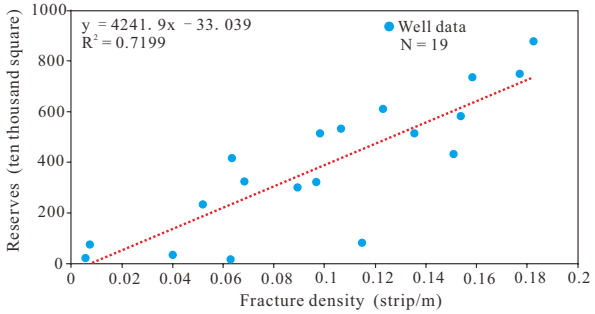


**Fig. 8**. Relationship between predicted fracture density and oil and gas reserves in Lower Wenchang period of Lufeng Depression.

principal stress in the lower Wenchang deposition period of the Lufeng Depression: the northwestern uplift zone, the eastern low uplift zone, and the southern steep slope zone of Lufeng 13 Sag, which all have relatively high structural positions; at the same time, there are two low-value areas of maximum principal stress: the Lufeng 13 east-west depression and the gentle slope belt in the north of Lufeng low-middle uplift. The minimum principal stress reaches the maximum value in the Dongsha uplift in the south of the Lufeng Depression, and it is low in the eastern gentle slope zone.

3) The quantitative fracture prediction findings indicate that the slope belt in the north of Lufeng 7 Sag, the Lufeng mid-low uplift in the north of Lufeng 13 east Sag, and the low uplift in the northwest of Dongsha uplift are the major fractured reservoir development sites. It was also confirmed that the technique of prediction is reasonable, with an average error of 13.61 percent. In the eastern portion of the Lufeng 13 Sag, the central portion of the Lufeng 7 Sag, and the certain areas of the Lufeng 15 Sag, the fracture development density is 0.12 to 0.18 strip/m, which represents relatively favorable fracture development conditions in comparison to other areas (fracture development density is 0.01 to 0.1 strip/m), which can provide ideal migratory patterns and reservoir conditions for the accumulation of nearby oil and is the

focus of the next phase of oil exploration.

## Acknowledgements

This study was supported by the Major National R&D Projects of China (No. 2016ZX05024-004) and the research project of CNOOC (Shenzhen) (No. SCKY-2020-SZ-21). The authors appreciate the efforts of CNOOC in providing experimental materials and their permission to publish this study.

## Conflict of interest

The authors declare no competing interest.



## References

Aydin, A. Failure modes of shales and their implications for natural and man-made fracture assemblages. AAPG Bulletin, 2014, 98(11): 2391-2409.

Baytok, S., Pranter, M. J. Fault and fracture distribution within a tight-gas sandstone reservoir: Mesaverde Group, Mamm Creek Field, Piceance Basin, Colorado, USA. Petroleum Geoscience, 2013, 19(3): 203-222.

Chen, Q., Fan, T., Li, X., et al. In situ measurements and comprehensive research on the present crustal stress of Northern South China Sea. Chinese Journal of Geophysics, 2014, 57(8): 2518-2529. (in Chinese)

Chen, J., Wang, L., Wang, C., et al. Automatic fracture optimization for shale gas reservoirs based on gradient descent method and reservoir simulation. Advances in Geo-Energy Research, 2021, 5(2): 191-201.

Cui, J., Tang, Z., Wang, L., et al. The spatial distribution of microfaults and the tectonic stress field analysis during brittle deformation of the main hole core at Chinese Continental Sciences Drilling (CCSD). Acta Petrologica Sinica, 2009, 25(7): 1619-1626. (in Chinese)

Cui, X., Xia, B., Zhang, Y., et al. A numerical modeling study on the "Asthenosphere Upwelling" of South China Sea. Geotectonica et Metallogenia, 2005, 29(3): 334-338. (in Chinese)

Curtis, J. B. Fractured shale-gas systems. AAPG Bulletin, 2002, 86(11): 1921-1938.

Ding, Z., Qian, X., Huo, H., et al. A new method for quantitative prediction of the tectonic fractures-two-factor method. Oil and Gas Geology, 1998, 19(1): 1-7. (in Chinese)

Feng, W., Wang, F. Guan, J., et al. Geologic structure controls on initial productions of Lower Silurian Longmaxi shale in south China. Marine and Petroleum Geology, 2018, 91: 163-178.

Gale, J. F. W., Laubach, S. E., Olson, J. E., et al. Natural fractures in shale: A review and new observations. AAPG Bulletin, 2014, 98(11): 2165-2216.

Islam, M. S., Shinjo, R., Kayal, J. R. The tectonic stress field and deformation pattern of northeast India, the Bengal basin and the Indo-Burma Ranges: A numerical approach. Journal of Asian Earth Sciences, 2011, 40(1): 121-131.

Kudrass, H. R., Wiedicke, M., Cepek, P., et al. Mesozoic and Cainozoic rocks dredged from the South China Sea (Reed Bank area) and Sulu Sea and their significance for plate-tectonic reconstructions. Marine and Petroleum Geology, 1986, 3(1): 19-30.

Lavrov, A. The Kaiser effect in rocks: Principles and stress estimation techniques. International Journal of Rock Mechanics and Mining Sciences, 2003, 40(2): 151-171.

Laurent, M., Frantz, M. Chronologic modeling of faulted and fractured reservoirs using geomechanically based restoration: Technique and industry applications. AAPG Bulletin, 2006, 90(8): 1201-1226.

Liao, Z., Cheng, C., Cheng, L., et al. Study on facies-controlled model of a reservoir in Xijiang 24-3 oilfield in the Northern Pearl River Mouth Basin. Advances in Geo-Energy Research, 2018, 2(3): 282-291.

Liu, J., Ding, W., Wang, R., et al. Simulation of paleotectonic stress fields and quantitative prediction of multi-period fractures in shale reservoirs: A case study of the Niutitang Formation in the Lower Cambrian in the Cen'gong block, South China. Marine and Petroleum Geology, 2017, 84: 289-310.

Liu, G., Lu, H., He. S., et al., Application of finite element analysis in a reservoir in situ-stress research. Science Technology and Engineering, 2009, 9(24): 7430-7435. (in Chinese)

Liu, C., Zhang, L., Martyushev, D. A., et al. Effects of microfractures on permeability in carbonate rocks based on digital core technology. Advances in Geo-Energy Research, 2022, 6(1): 86-90.

Nelson, R. A. Geologic analysis of Naturally Fractured Reservoirs. Amsterdam, the Netherlands, Elsevier, 2001.

Nissen, M. T., Fournier, A., Dahlen, F. A. A two-dimensional spectral-element method for computing spherical-earth seismograms–I. Moment-tensor source. Geophysical Journal International, 2007, 168(3): 1067-1092.

Olson, J. E., Laubach, S. E., Lander, R. H. Natural fracture characterization in tight gas sandstones: Integrating mechanics and diagenesis. AAPG Bulletin, 2009, 93(11): 1535-1549.

Price, N. J. Fault and Joint Development in Brittle and Semi-brittle Rock. Amsterdam, the Netherlands, Elsevier, 2016.

Rajabi, M., Sherkati, S., Bohloli, B., et al. Subsurface fracture analysis and determination of in-situ stress direction using FMI logs: An example from the Santonian carbonates (Ilam Formation) in the Abadan Plain, Iran. Tectonophysics, 2010, 492(1): 192-200.

Ross, A. R., Brown, L. D., Pananont, P., et al. Deep reflection surveying in central Tibet: Lower-crustal layering and crustal flow. Geophysical Journal International, 2004, 156(1): 115-128.

Wang, X., Zhang, X., Lin, H., et al. Paleogene geological framework and tectonic evolution of the central anticlinal zone in Lufeng 13 sag, Pearl River Mouth Basin. Petroleum Research, 2019, 4(3): 238-249.

Westaway, R., Maddy, D., Bridgland, D. Flow in the lower continental crust as a mechanism for the Quaternary uplift of south-east England: Constraints from the Thames terrace record. Quaternary Science Reviews, 2002, 21(4): 559-603.

Wu, L., Liu, C., Zhang, T., et al. The application of two factor method in quantitative prediction of tectonic fractures: A case study of shale in QING-1 member, Songliao Basin, Journal of Geomechanics, 2018, 24(5): 598-605. (in Chinese)

Yu, F., Koyi, H. A., Zhang, X. Intersection patterns of normal faults in the Lufeng Depression of Pearl River Mouth Basin, China: Insights from 4D physical simulations. Journal of Structural Geology, 2016, 93: 67-90.

Zeng, H., Song, H. A study on 3-D finite element inverse model. Journal of Geomechanics, 1999, 5(1): 45-49. (in Chinese)